Computers & Fluids 49 (2011) 312–322

Contents lists available at ScienceDirect

Computers & Fluids

journal homepage: www.elsevier.com/locate/compfluid

Hybrid simulations of rarefied supersonic gas flows in micro-nozzles

F. La Torre [a], S. Kenjereš [a], J.-L. Moerel [b], C.R. Kleijn [a,*]

[a] Department of Multi-Scale Physics, Faculty of Applied Sciences, Delft University of Technology, Prins Bernhardlaan 6, 2628 BW Delft, The Netherlands
[b] Department of System Performance and Survivability, TNO Defence, Security and Safety, P.O. Box 45, 2280 AA Rijswijk, The Netherlands

ARTICLE INFO

Article history:
Received 1 November 2010
Received in revised form 6 June 2011
Accepted 17 June 2011
Available online 29 June 2011

Keywords:
Micro-thruster
Micro-nozzle
DSMC
Hybrid methods
Rarefied flow
Supersonic flow

ABSTRACT

We show that accurate predictions of gas flow and pressure in axisymmetric micro-thruster nozzles with throat diameters in the μm range, and thrusts in the μN range, cannot be performed using continuum based Computational Fluid Dynamics with slip flow boundary conditions, but can be performed by applying a static, one-way, state-based coupling between a CFD solver applied upstream from a properly chosen cross sectional (perpendicular to the nozzle axis) interface, and a Direct Simulation Monte Carlo solver applied downstream from that interface. These hybrid CFD/DSMC simulations can be performed in 5–25% of the CPU time required for a full DSMC simulation, with an accuracy better than 1–2%. A non-optimal choice of the interface location may increase the errors up to several tens of percents, when the interface is located too far downstream, or increase the CPU time by up to several tens of percents, when the interface is located too far upstream. The proper interface location does not generally coincide with the throat plane, but lies upstream or downstream from the throat, depending on the flow conditions. We provide a quantitative criterion, based on Knudsen numbers as estimated from full CFD simulations of the entire nozzle, to determine the proper interface location *a priori*. Due to frictional losses and rarefaction effects, the total thrust of micro-nozzles in the μN range is found to be several tens of percents lower than the thrust predicted from one-dimensional isentropic theory.

© 2011 Elsevier Ltd. All rights reserved.

1. Introduction

For the development of so-called micro-satellites (which have a typical volume of 1 dm^3), existing propulsion systems, with thrusts T in the kN–MN range, are too large and too heavy. The required thrust to maintain or adjust the orbit of micro-satellites, or to provide them with long duration low thrust acceleration, is in the μN–mN range. One of the simplest forms of micro-propulsion is the cold gas thruster: the gas, pressurized in a microtank, is accelerated and expanded through a convergent–divergent nozzle. With the characteristic dimensions of the nozzle (*e.g.* the throat diameter $2R_t$) being proportional to $\sqrt{T}$, micro-thruster nozzles have typical throat diameters in the μm–mm range, and are being manufactured using MEMS technology [1–3].

Whereas large scale nozzles can be accurately designed based on one-dimensional isentropic flow theory [4], such an approach fails for the design and analysis of micro-nozzles since: (1) for the reduced Reynolds numbers that prevail in micro-nozzles ($Re \sim \sqrt{T}$), the thickness of the hydrodynamic boundary layers is no longer negligible compared to the nozzle diameter, and frictional losses significantly reduce thrust [5]; (2) the surface roughness that is introduced by typical MEMS manufacturing technologies can be relatively large compared to the nozzle dimensions, introducing further loss in thrust [5]; and (3) due to the small dimensions, rarefaction effects play an important role. As a consequence of all of this, multi-dimensional numerical simulations, based on realistic flow models including compressibility, viscous losses and rarefaction, must be used to design and analyse the gas flow in micro-nozzles. This is not a trivial task, particularly because of the transition from continuum to rarefied flow regimes inside the nozzle, requiring the use of hybrid simulation methods. This paper focuses on the efficient, consistent and accurate use of hybrid methods to simulate all gas flow regimes in micro-nozzles, addressing several issues that have remained under-exposed so far in literature.

When operated in space, the pressure in micro-nozzles varies from several bars in the gas chamber and the convergent, to several millibars in the divergent, to near vacuum in the plume far away from the nozzle exit. Correspondingly, the molecular mean free path λ varies from tens of nanometers, to tens of microns, to millimetres. Consequently, the gas flow in micro-nozzles experiences changes from the continuum regime (Knudsen number $Kn < 0.01$) in the gas chamber and the convergent part of the nozzle, to the slip flow and transition regimes ($0.01 < Kn < 0.1$ and $0.1 < Kn < 10$, respectively) in the divergent part of the nozzle, up to the free molecular regime ($Kn > 10$) far from the exit of the nozzle. Here, the Knudsen number is defined as the ratio between the molecular mean free path and some characteristic macroscopic length scale ℓ

* Corresponding author. Tel.: +31 15 2782835; fax: +31 15 2782838.
E-mail address: C.R.Kleijn@tudelft.nl (C.R. Kleijn).

0045-7930/$ - see front matter © 2011 Elsevier Ltd. All rights reserved.
doi:10.1016/j.compfluid.2011.06.008

$$Kn = \frac{\lambda}{\ell} \quad (1)$$

It is generally known that important deviations from continuum flow occur in the vicinity of solid walls at Knudsen numbers larger than ~0.1. Therefore, some attempts have been made to use Navier–Stokes equations with slip wall boundary conditions to model micro-nozzle gas flows, for example in [6–10]. However, such an approach is known not to be accurate when the Knudsen number exceeds 0.1, see *e.g.* [11,12]. Moreover, rarefaction effects in micro-nozzles do not only – and, as will be shown later in this paper, not even primarily – take place in the vicinity of the walls. In the region of sonic transition in and behind the throat, extremely sharp changes in temperature, pressure and velocity occur in the bulk of the flow, over distances of just a few mean free paths.

It is therefore generally assumed that the accurate modelling of gas flows in micro-nozzles requires the use of non-continuum flow models. In the transition regime, the most accurate method to use is Direct Simulation Monte Carlo (DSMC) [13], which was shown to provide accurate solutions for highly rarefied nozzle and plume flows first in [14]. DSMC is more efficient than deterministic molecular models such as Molecular Dynamics (MD), and more flexible and generally applicable than methods based on direct solution of the Boltzmann or BGK equations [10]. DSMC simulations for different micro-nozzle configurations were performed in [10,15–19].

In principle, DSMC is valid for all flow regimes. However, in order for its solutions to be accurate, the requirements on the grid size and time step size increase severely with decreasing Knudsen number, both being proportional to Kn^{-1}. Since the total number of particles scales proportionally with the number of grid cells, the computational expenses of a proper DSMC simulation scale with Kn^{-4}. In practice, an accurate DSMC solution in the low *Kn* number regions is therefore extremely costly, and the application of DSMC to an entire micro-nozzle flow is not generally feasible. In this context it should be noted that the above references pay little, if any, attention to the required accuracy of the obtained DSMC solutions in the low *Kn* number regions of the nozzle.

To overcome this problem, a hybrid continuum/DSMC model can be considered. The method applies the continuum approach in low *Kn* regions, while DSMC is applied in regions where rarefaction effects need to be considered. A discussion on the major considerations involved with hybrid models and a summary of the state-of-art is provided by Wu and coworkers and by Wijesinghe and Hadjiconstantinou in [20,21]. Different hybrid models have been proposed to couple DSMC and Stokes equations [22], DSMC and incompressible Navier–Stokes equations [21], DSMC and Euler equations [21,23–25], and DSMC and Navier–Stokes equations [26–32].

One of the main issues in such techniques is the way in which the transfer of information between particle and continuum domains is handled. In general, two main approaches can be distinguished [28,29]: a flux-based coupling, where fluxes of mass, momentum and energy are computed at the interface, and a state-based coupling, for which average particle information results in a macroscopic state on one side of the interface and a distribution of particles is generated from a macroscopic state on the other side of the interface. It has been pointed out that the latter not only reduces the statistical noise associated with the flux quantities [21,33], but also allows for a conservative formulation of the fluxes into both the domains [29]. This approach was followed, for example, in [23,24,27,34,35] for different applications.

Another issue is the precise location of this interface. This can be determined dynamically, *e.g.* based on the local value of the Knudsen number [28,36,37], or statically, based on some a priori knowledge about the flow characteristics [15,19,35].

In the present paper, a one-way, state-based coupling from compressible Navier–Stokes based CFD to DSMC will be used to study the gas flow expanding through convergent–divergent micro-nozzles from high inlet pressure to vacuum. Such an approach was occasionally used for micro-nozzle flows, *e.g.* in [19], where the interface between CFD and DSMC was set at the throat of the nozzle and ideal sonic conditions were assumed at this location, and in [15], where CFD was applied throughout the nozzle and DSMC was applied to the plume. Whereas in all mentioned cases the location of the interface was fixed, it remained unclear whether this was indeed done at the optimum location, both with respect to accuracy and computational requirements. Obviously, both the total computational effort and the accuracy decrease when the interface is located further downstream.

The novelty of the work presented in the present paper lies in the fact that we quantify how the location of the interface between CFD and DSMC influences the accuracy and the computational requirements of the hybrid solution, and that we formulate a general criterion that can be used to *a priori* determine the optimum location of the interface. Both these important aspects have not been addressed earlier in the simulation of micro-nozzle gas flows.

In order to do so, we study four different micro-nozzle configurations in the μN thrust range, with varying dimensions, inlet pressures and divergent angles. We start by performing full DSMC simulations of the entire nozzle. Unlike most literature on the use of DSMC in micro-nozzles, we present a detailed analysis on the numerical accuracy of our solutions, showing that they have converged with respect to grid size, time step size, and number of simulated particles. These accurate full DSMC solutions are then used as benchmark against which we validate both full Navier–Stokes solutions with slip flow boundary conditions, and hybrid Navier–Stokes/DSMC solutions. In the latter, we put the interface between CFD and DSMC at a large number of different cross sections perpendicular to the nozzle axis, both upstream, at, and downstream from the throat.

After a brief introduction on the studied problem (Section 2), the numerical methods and accuracy will be discussed in the Section 3, while the numerical results will be shown in Section 4. Our general conclusions as to the optimum location of the interface in hybrid CFD/DSMC simulations of micro-nozzles will be formulated in Section 5.

2. Nozzle flow simulations

The studied 2D axisymmetric nozzle is shown in Fig. 1. Such conical micro-nozzles can now be fabricated in MEMS technology, and are typical for micro-nozzle thrusters as used in practice [1–3]. Two different regions can be distinguished: a convergent part, where the flow is accelerated from the initial subsonic velocity to the sonic condition (which is reached at the throat), and a divergent part, where the flow expands to the outlet in a supersonic regime.

The four considered configurations are summarized in Table 1, where the ideal thrust T_{ideal} is computed from the 1D isentropic flow theory and the throat Knudsen number Kn_t is computed from the average mean free path at the throat, and the throat radius as characteristic length.

Although, for a given gas (*i.e.* given Prandtl number and specific heat ratio) and under ideal gas assumptions, the gas flow is fully determined by the Reynolds and Mach numbers, the choice of the four mentioned configurations was primarily based on the variation of the throat Knudsen number, which is proportional to the ratio of Mach and Reynolds, in the 0.01–0.1 region. Starting from configuration 1 with $Kn_t = 0.008$, we increased Kn_t by decreasing the characteristic length of the problem (configuration 2) and

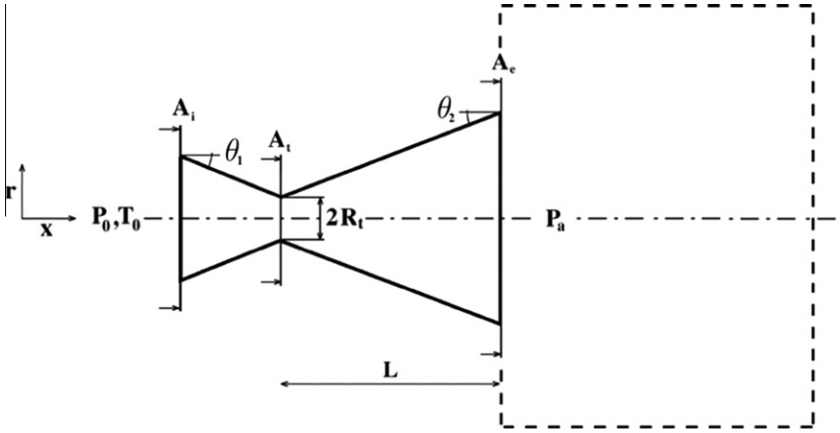

Fig. 1. Studied nozzle geometry, with the problem parameters of interest. The computational domain was extended to include the so-called plume area, the boundaries of which are indicated with the dashed lines. In the DSMC and hybrid simulations, a vacuum boundary condition was imposed on these boundaries, whereas in the CFD simulations, a zero far field pressure boundary condition was imposed.

Table 1
Definition of the four studied micro-nozzle configurations. Inlet pressure P_0, throat radius R_t, divergent angle θ_2, ideal thrust T_{ideal} and throat Knudsen number Kn_t. Also shown are the number of computational particles $\overline{N_P}$, the time step size $\overline{\Delta t}$, and the number of DSMC iterations N_{it} for the full DSMC simulations, as well as their total CPU times. It should be noted that CPU times for full CFD simulations are only a few hours, whereas hybrid CFD/DSMC simulations have CPU times that are only 5–25% of the full DSMC simulations.

Configuration	P_0 (Pa)	R_t (μm)	θ_2 (°)	T_{ideal} (μN)	Kn_t	$\overline{N_P}$	$\overline{\Delta t}$	N_{it}	CPU time (h)
1	3.5×10^5	3.56	20	25.0	0.008	20.0×10^6	1.2×10^{-11}	130,000	4200
2	3.5×10^5	1.13	20	2.5	0.025	14.0×10^6	7.0×10^{-12}	130,000	2000
3	0.5×10^5	3.56	20	3.6	0.055	7.0×10^6	2.0×10^{-11}	80,000	650
4	0.2×10^5	3.56	30	1.4	0.125	2.0×10^6	5.0×10^{-11}	60,000	250

increasing the mean free path in the flow (configuration 3). In configuration 4, a very low inlet pressure was imposed. For such a low pressure, due to the formation of thick viscous boundary layers and the consequent smaller available area for expansion, a wider divergent angle is needed to allow for a supersonic expansion in part of the nozzle divergent [3]. Therefore, for configuration 4 we used a divergent angle of 30°, and a shorter divergent length to obtain the same exit flow area as in previous cases. By inclusion of test case 4, we will show the geometry independence of our results.

A sharp angle is considered to connect the convergent and the divergent, as is found in the experimentally fabricated micro-nozzles [1–3]. Although such a sharp angle creates some additional non-equilibrium effects, its advantage is that a shorter divergent length can be used for a fixed exit diameter, leading to reduced friction losses. All the configurations have an inlet area equal to 7.27 times the throat area, and an outflow area of 23.23 times the throat area. In the inlet, nitrogen gas is introduced at a fixed temperature of 300 K and pressure P_0 varying according to Table 1. The computational domain extends far downstream from the divergent exit, to include the so-called plume area, as indicated by the dashed lines in Fig. 1. At these far-field boundaries, vacuum (zero pressure) conditions are assumed. The walls are modelled as isothermal at a temperature of 300 K.

The performance of the nozzle, as resulting from the different numerical approaches, is evaluated through the thruster relative efficiency, defined as:

$$\eta = \frac{T_{real}}{T_{ideal}} \tag{2}$$

The ideal thrust T_{ideal} is given by the 1D isentropic flow theory [4]. Under continuum assumptions, the real thrust T_{real} is computed from:

$$T_{real} = \int_{A_e} [\dot{m} V_e + (p_e - p_a)] dA \tag{3}$$

where $\dot{m}$ is the mass flow rate, the subscript e refers to the conditions at the exit of the nozzle and the subscript a refers to the ambient conditions outside the nozzle. For the strongly non-equilibrium conditions that are present in micro-nozzles under rarefied conditions, the pressure tensor will be anisotropic. Rather than applying continuum assumptions, the flow in the outlet will be modelled using particle based Direct Simulation Monte Carlo techniques, as discussed in the following section. The thrust is then directly computed from the momentum flux of particles across the nozzle exit plane.

Eq. (3) shows that the total thrust is composed of two terms: the first one, which we will call the *jet thrust* T_{jet}, is proportional to the mass flow and the exit velocity and is generally (much) larger than the second one, the *pressure thrust* T_{press}, which depends on the exit and ambient pressures. As will be shown later (see *e.g.* Fig. 9), this even is the case for micro-nozzles operated in zero ambient pressure, as studied in this paper.

3. Numerical approach

3.1. The CFD solver

All CFD simulations have been obtained with the general purpose code Fluent, version 6.3 [38]. The solved equations included the continuity equation, the Navier Stokes equations in compressible form, and the thermal energy equation. Nitrogen was treated as an ideal gas, with temperature dependent viscosity and thermal conductivity computed from kinetic theory [39], using the Lennard–Jones parameters $\sigma = 3.621$ Ång and $\epsilon/k = 97.53$ K for Nitrogen gas. The studied nozzle has a conical shape and therefore a 2D-axisymmetric flow was considered. At the nozzle walls, slip wall boundary conditions according to the formulas by Maxwell [40] and von Smoluchowski [41], assuming fully diffusive walls, were applied. At the exit boundaries of the extended computa-

tional domain, a zero far field pressure boundary condition was imposed. The local mean free path λ is computed from the local temperature and pressure as calculated with the CFD solver as $\lambda = k_B\Theta/\left(\pi\sqrt{2}d_{ref}^2P\right)$, where d_{ref} is the diameter of gas particles and Θ is the temperature.

Slip flow boundary conditions are provided in Fluent, but cannot be combined with its fully coupled compressible solver. Therefore, we have implemented the slip flow boundary conditions through a User Defined Function (UDF), which is compatible with the coupled compressible solver. The use of more advanced slip boundary conditions [42,43] will be discussed in Section 4.1. Downstream of the nozzle exit, an outflow area, or plume region, with a width and length much larger than the nozzle exit diameter was added to the computational domain, and a far-field vacuum condition was imposed on the boundaries of this area. It was checked that the flow characteristics inside and at the exit of the nozzle were not significantly influenced by the precise dimensions of this plume region.

The computational grid, generated with Gambit [44], consisted of roughly uniformly sized quadrilateral elements, with 100 grid cells in the radial direction and about 600 grid cells in the axial direction in the nozzle domain, and 15,000 additional grid cells in the plume region.

The equations were discretized in space using a second order upwind scheme, and solved using Fluent's implicit coupled density based solver. The accuracy of the numerical solution has been tested by comparing, for configuration 1, results obtained with first-, second-, and third-order spatial discretization schemes, and different meshes, doubling and quadrupling the number of cells in each direction. Negligible differences were observed between the various discretization schemes and grids.

3.2. Direct simulation Monte Carlo

The DSMC method is comprehensively described by Bird in [13]. It is not based on solving partial differential equations, but describes the state of the system by computing the positions and velocities of computational particles, each of which represents an assigned number of particles in the real flow. The computational domain is divided into grid cells, through which the particles can move. All the properties of the particles are stored and updated each time step during the calculation. In each time step, first the particles are moved as if they did not interact, and any particles that reach a boundary are processed according to the appropriate boundary condition. Second, after all the particles have moved, a certain number of particles from each grid cell are randomly selected for collisions, and these collisions are treated according to one of the collisions models described by Bird in [13].

The DSMC solver used in the present study was the general purpose DSMC code X-Stream/DSMC [45], which can handle 3-D boundary fitted structured meshes and has been validated for a wide range of problems [46], amongst which the case of a low pressure micro-nozzle as studied in [17]. In all the simulations presented in this paper, a Variable Soft Sphere (VSS) model has been used, with the corresponding parameters $\Theta_{ref} = 273$ K, $\omega = 0.74$, $\alpha = 1.36$ and $d_{ref} = 4.11 \times 10^{-10}$ m for Nitrogen from [13]. This combination of VSS parameters provides viscosities and thermal conductivities that are consistent with the values computed from kinetic theory used in the CFD simulations.

The interaction between the particles and the walls was modelled as fully diffusive. At the exit boundaries of the extended computational domain, a vacuum boundary condition was imposed, *i.e.* particles crossing these planes are removed from the simulations. In order to model axial-symmetry, to each particle a radial weighting factor, depending on the radial position of the cell in which it resides, has been assigned, as described in [13,46]. In this way, a particle located far from the axis represents a larger number of real molecules than one near the axis. It was shown by Bird in [13] that considering the same weighting factor for all the particles within a cell, rather than using a continuous weighting factor, has negligible effects on the flow solution.

In order to produce accurate results, the DSMC method implies restrictions to the time step size, grid cell size and number of simulated particles [13,47,48]. The decoupling between the translational movement of the particles and their collisions is accurate only when the time step is a small (typically $\ll 1$) fraction of the mean collision time. Similarly, the random selection of the particles from a grid cell as possible collision partners leads to the restriction that the grid cell size needs to be a small (typically <1/3) fraction of the molecular mean free path. Finally, the number of particles per cell needs to be high enough (typically >15–20) to avoid repeated collisions between the same particles and make the collision process statistically accurate. Although it has been shown [49,50] that the mentioned restrictions can be somewhat relaxed under specific conditions, for instance using cell sizes larger than the local mean free path in directions where gradients are small, and although DSMC algorithms have been recently improved for performance [51,52], particularly the constraints on grid cell size and number of particles per cell make DSMC computationally expensive for small Knudsen number flows.

In the present study, for the four configurations in Table 1, we performed an extensive analysis of the sensitivity of our DSMC simulation results to the grid cell size, time step size and number of particles per cell. Fig. 2 shows results of a grid cell size sensitivity study for configuration 2. Exit velocity and pressure profiles from full DSMC simulations, obtained on different grids, show that an accurate solution is obtained on the one but finest of the considered meshes. Fig. 3 shows results of a sensitivity study with respect to the time step size and the number of simulated particles for configuration 3. Starting from base values $\overline{\Delta t}$ for the time step and $\overline{N_P}$ for the number of particles (which were both chosen in agreement with the general DSMC guidelines described above) we multiplied the time step by factors 0.5, 2 and 4, and the number of particles by factors 0.25, 0,5 and 2. Neither halving the time step, nor doubling the number of particles, leads to a significant change in the exit velocity profiles (and pressure profiles, not shown) compared to using the base values. All results presented further in this paper have similarly been shown to be independent of the grid cell size, time step size and number of computational particles. The simulations involved from $\sim$2 millions of computational particles for configuration 4, to $\sim$20 millions of computational particles for configuration 1. All the cases were solved on a 16 processors Linux cluster with an overall memory of 64 Gb. Mentioned CPU times are summed over all CPU's.

3.3. The hybrid CFD/DSMC approach

In the upstream, high pressure, part of the nozzle, it is not necessary to account for rarefaction effects, since the local Knudsen number is very low. Therefore, in order to overcome the problems related to the enormous computational time required by accurate full DSMC simulations, a hybrid Navier–Stokes/DSMC model is the obvious approach to consider. Here, one applies the DSMC method only in those regions where rarefaction effects are important. In the present paper, we use a one way (single step), state-based coupling from CFD to DSMC, applying CFD with slip flow boundary conditions in a region upstream of a certain cross section of the nozzle, and DSMC in a the remaining part downstream from that cross section. Apart from the advantages of state-based coupling methods in general, as mentioned earlier, our choice for the way in which the two methods are coupled is based on its simplicity, which allows the easy transfer of information between two inde-

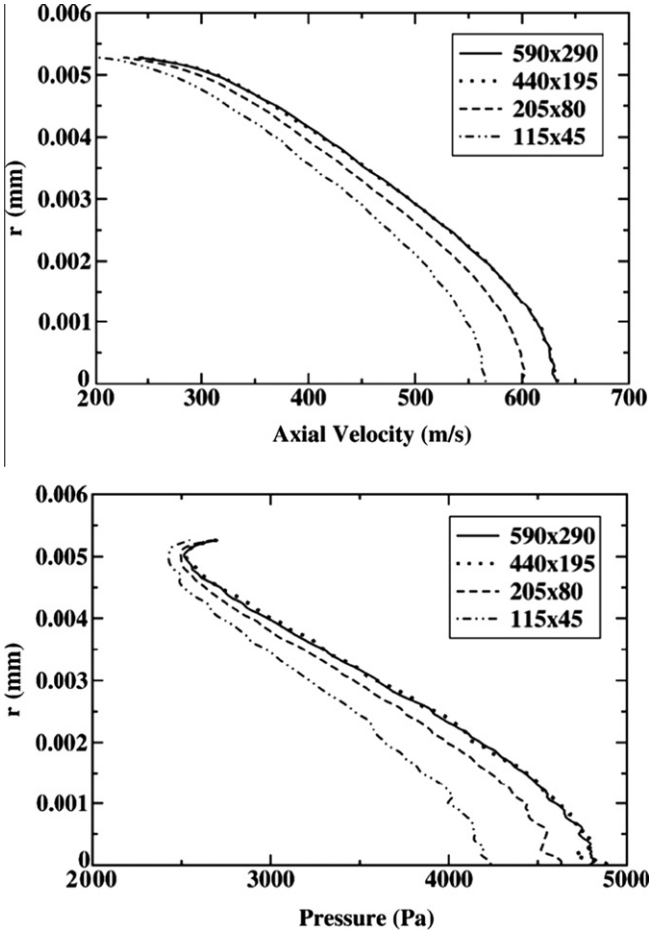

Fig. 2. Exit velocity (top) and exit pressure (bottom) profiles obtained with full DSMC simulations on different grids for configuration 2. The number of computational particles varied from 1.5 million on the coarsest, to 14 million on the finest mesh. The total CPU time varied from 80 h on the coarsest, to 2000 h on finest mesh.

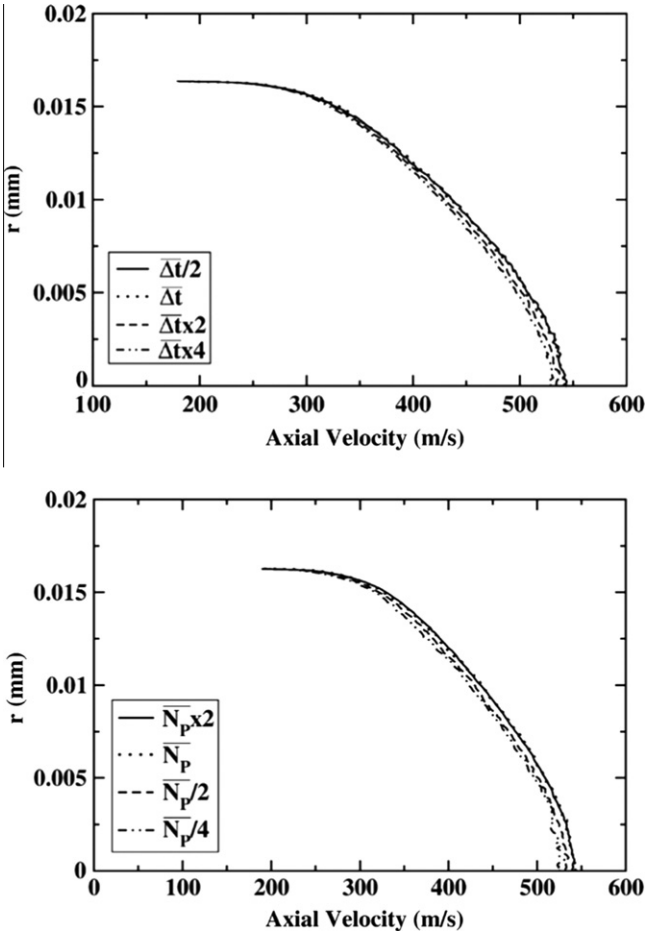

Fig. 3. Exit axial velocity profiles obtained from full DSMC simulations with different time step sizes (top) and number of computational particles (bottom) for configuration 3. Starting from base values $\overline{\Delta t}$ for the time step and $\overline{N_P}$ for the number of particles (which were both chosen in agreement with the general DSMC guidelines described in the main text) we multiplied the time step by factors 0.5, 2 and 4, and the number of particles by factors 0.25, 0, 5 and 2. Neither halving the time step, nor doubling the number of particles, leads to a significant change in the results compared to using the base values.

pendent, stand alone (possibly commercial) solvers, for CFD and DSMC respectively.

At the cross-sectional interface, which is perpendicular to the nozzle axis, a Dirichlet–Dirichlet boundary condition is applied. First, a CFD simulation (with slip wall boundary condition) is run to estimate the solution in the entire domain. Second, the cross-sectional interface is fixed on a certain position along the axis of the nozzle, and the CFD solution at that interface is imposed as inlet boundary condition for the DSMC simulation, downstream from the interface. In the DSMC cells directly adjacent to the interface, DSMC particles are created according to the density, velocity, and temperature of the CFD solution.

Here, care should be given as to the velocity distribution of these particles. Whereas most DSMC simulations apply (inflow) boundary conditions in uniform flow regions, where a Maxwellian distribution is the obvious and physically correct choice [29], there is less consensus as to which distribution should be used at the Navier Stokes–DSMC interface in a hybrid simulation. From a formal viewpoint, the Chapman–Enskog distribution would be the better choice, since, unlike the Maxwell distribution, it is consistent with the Navier–Stokes equations [26,29,64]. Indeed, it has been shown that the use of a Chapman–Enskog distribution leads to somewhat higher accuracy as compared to a Maxwellian distribution in hybrid DSMC–Navier Stokes simulations of a Couette flow, which is an extreme example of a strongly non-equilibrium flow driven purely by gradient effects [58]. Based on these findings, many recent papers on hybrid DSMC–Navier Stokes simulations have applied a Chapman–Enskog distribution [29,31,61,20,63,62]. Other authors, on the other hand, have chosen to apply a Maxwellian distribution in hybrid DSMC–Navier Stokes simulations, arguing that the use of a Chapman–Enskog distribution leads to a small improvement in accuracy [59,65] which does not justify the largely increased computational costs [60], or because of the fact that the Chapman–Enskog distribution becomes negative with deviation from the Maxwellian distribution [59], or because of the observation that for specific flows a greater mismatch at the interface between Navier Stokes and DSMC was observed for a Chapman–Enskog distribution as compared to a Maxwellian distribution [64].

In the present study we apply a simple, static, one-way coupling between a commercial CFD solver used upstream from the cross-sectional interface, and a commercial DSMC solver used downstream from that interface. The CFD results at the interface are fed into the DSMC code as inflow boundary conditions. As a consequence, the DSMC particles at the interface have been generated according to a Maxwellian distribution. Fig. 4 shows profiles of the gas velocity, pressure and density along the nozzle axis for a hybrid simulation of case 2 from Table 1, compared to the corresponding profiles for a full DSMC solution. This demonstrates that, for the studied supersonic nozzle flows and the applied location and orientation of the interface, our coupling scheme produces a very smooth transition between CFD and DSMC with negligible

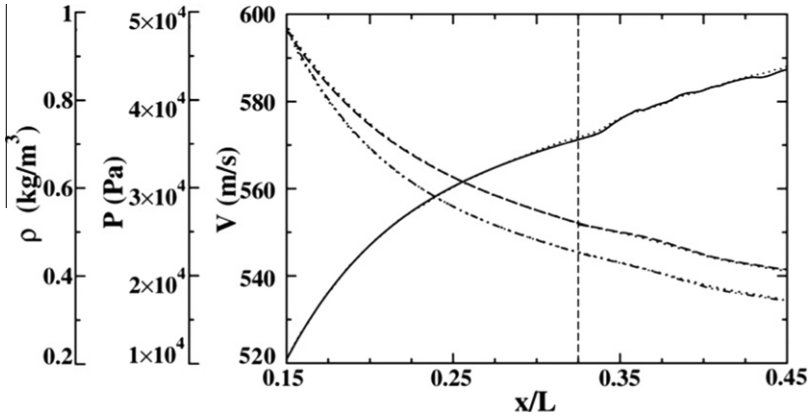

Fig. 4. Profiles of the gas velocity (continuous line), pressure (dash dot dot line) and density (dashed line) along the nozzle axis for a hybrid simulation of case 2 from Table 1, with the coupling interface, as indicated by the vertical dashed line, located at $x/L = 0.325$. Also shown are the corresponding profiles (dotted lines) from a full DSMC solution. A very smooth transition, with negligible mismatch, is observed across the interface, as well as very small differences compared to the full DSMC solution.

mismatch is across the interface, as well as very small differences between hybrid and full DSMC solutions, despite of the use of the less accurate Maxwell distribution.

4. Results

4.1. Comparison between full CFD and full DSMC solutions

Fig. 5 shows a first comparison between the solutions obtained from a full CFD simulation, with velocity and temperature slip wall boundary conditions, and the solutions from full DSMC, for all the four test cases.

In general, the DSMC solution predicts a larger expansion of the flow, with a correspondingly higher velocity and lower pressure in the outlet, than the CFD results. This under-prediction of the expansion by CFD increases with increasing Kn_t, when rarefaction effects start to appear already further upstream, *i.e.* shortly after the throat, or even upstream from the throat.

For case 1, with $Kn_t = 0.008$, a reasonable agreement is still found between the CFD solution with slip wall boundary conditions and the full DSMC solution. Nevertheless, the CFD solution under-predicts the Mach number in the outflow by some 5%. For case 2, with $Kn_t = 0.025$, CFD under-predicts the maximum Mach number in the outflow by some 25%. The differences get even larger in the cases 3 and 4 with reduced inlet pressure, in which

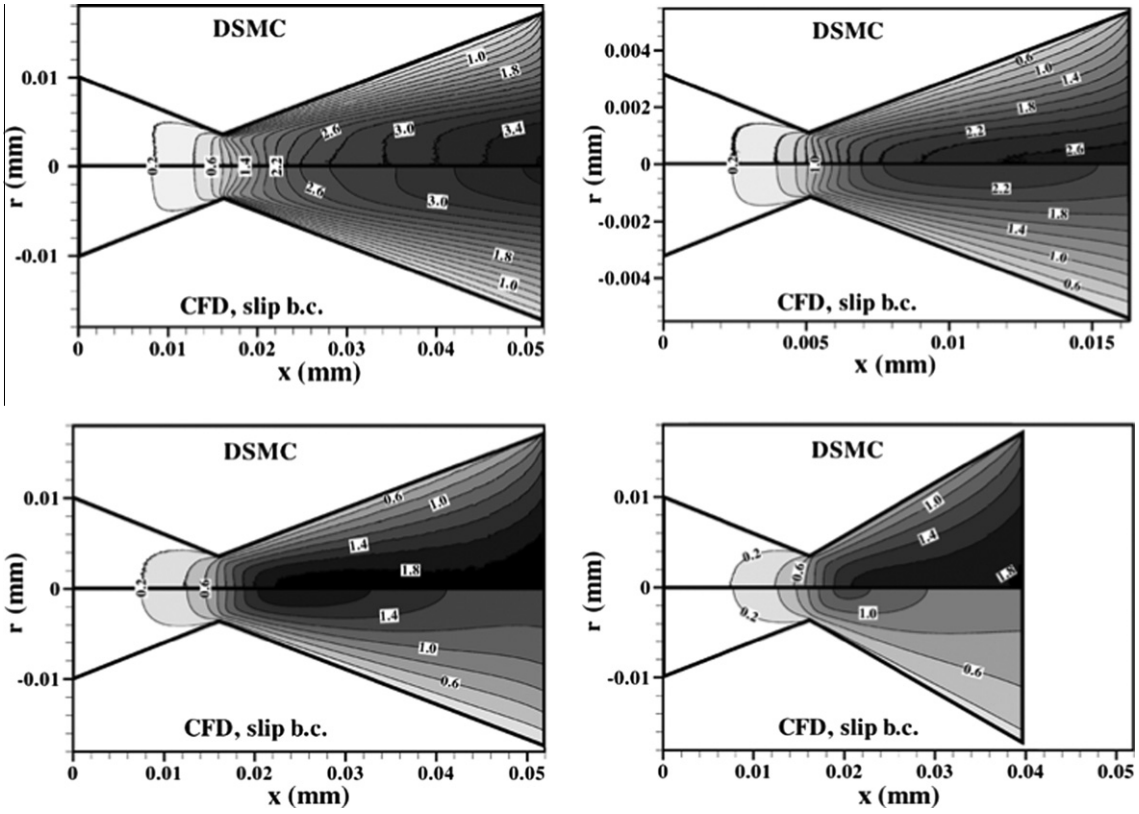

Fig. 5. Comparison of Mach number contours from the solution obtained by full DSMC (upper half pictures) and full CFD (lower half pictures), for the configurations 1 ($Kn_t = 0.008$, upper left), 2 ($Kn_t = 0.025$, upper right), 3 ($Kn_t = 0.055$, bottom left) and 4 ($Kn_t = 0.125$, bottom right), as listed in Table 1.

Kn_t = 0.055 and Kn_t = 0.125, respectively. Here, a supersonic region and further expansion of the gas flow are still present in the DSMC solution, whereas they are completely absent in the CFD solution. In the CFD simulations of these high Knudsen number cases, slip flow is under-estimated even though slip flow boundary conditions are used. As a result, thick hydrodynamic boundary layers develop, which slow down the flow to subsonic speeds. It should be noted here that the comparison between CFD and DSMC becomes even far worse when no-slip boundary conditions are used [53], leading to an even increase of the thickness of the subsonic boundary layer in the divergent, and a consequent even lower exit velocity.

From the above it may be concluded that full CFD solutions, even if thermal and velocity slip flow boundary conditions are applied, lead to large errors in the simulation of micro-nozzle flow when the throat Knudsen number is larger than ~0.01.

One might expect, as is commonly seen in CFD simulations of wall-bound weakly rarefied gas flows, that a better agreement between CFD and DSMC solutions could have been obtained if properly tuned slip flow parameters would have been used in the CFD simulations. To further elucidate on this, we have performed an extensive parameter optimization study on the thermal and velocity accommodation coefficients used in the CFD solutions, varying both of them independently in the 0.1–1 range. It was found to be impossible to match the CFD solutions to the DSMC solutions for any combination of accommodation coefficients. In fact, the results presented above, with both the thermal and the velocity accommodation coefficient in CFD set to 1.0, represent the best comparison to the DSMC solutions.

Obviously, more advanced slip flow models than those proposed by Maxwell and von Smoluchowski have been developed, as *e.g.* described by Sharipov in [42,43], and one might argue that using these could lead to better agreement between CFD and DSMC results. To test this, we performed CFD solutions in which the local temperature and velocity slip as obtained from DSMC were imposed as a boundary condition to the CFD solution. This may be viewed as a CFD simulation with the perfect slip boundary condition. However, even this did not lead to a satisfactory agreement between DSMC and CFD, the latter was still strongly under-predicting the flow expansion in the divergent.

It is therefore safe to conclude that, in agreement with what was found by Hamel for free jets [54], the gas flow in micro-nozzles with throat-based Knudsen numbers $Kn_t > 0.01$ are strongly influenced by rarefaction effects in the core of the expanding flow, *i.e.* in the sonic region and the supersonic region behind it. These effects cannot be accounted for by continuum based flow solvers, even when advanced slip wall models are used. Instead, non-continuum solvers should be applied in at least part of the nozzle.

4.2. Comparison between hybrid CFD/DSMC and full DSMC solution

The above showed the necessity of applying a non-continuum solver in that part of the nozzle where rarefaction plays an important role. It also showed that full DSMC solutions are extremely computationally demanding, particularly for smaller Kn_t. In this section we will therefore evaluate the accuracy and efficiency of the hybrid CFD/DSMC solver, focusing on the optimum choice of the location x_{int} of the cross sectional interface between the CFD and the DSMC region.

From the full CFD solutions with thermal and velocity slip wall boundary conditions, we calculated the maximum continuum breakdown parameter $Kn_{max}(r, x)$, locally defined at location (r, x) as the maximum Knudsen number, based on the *local* gradient length scales of the pressure P, density ρ, and temperature Θ [55]:

$$Kn_{max}(r,x) = \max_{\phi=P,\rho,\Theta}\left[\frac{\lambda}{\phi(r,x)}|\nabla\phi(r,x)|\right] \tag{4}$$

Several other continuum breakdown parameters have been suggested in literature [56,57], but the advantage of the maximum gradient based Knudsen number is that it can easily be estimated *a priori* from continuum CFD simulations, without prior knowledge as to the local degree of non-equilibrium.

This is displayed in Fig. 6 for all the four considered configurations. In all cases, Kn_{max} is very small in the nozzle inlet and remains small throughout a large part of the convergent. However, already upstream from the throat it starts to increase due to the sharp pressure and temperature gradients in that region and corresponding small gradient length scales. Downstream from the throat, Kn_{max} further increases.

It is clear that local Knudsen numbers reach higher values than the throat Knudsen number Kn_t, not only in the regions close to the wall, but also in the core of the expanding gas.

Already for case 1, which is characterized by a throat Knudsen number Kn_t = 0.008, local Knudsen numbers exceeding 0.1 are found in the divergent. It is to be expected, that accurate solutions require the use of DSMC in those parts of the nozzle where Kn_{max} is high.

The maximum local Kn number on a cross section at location x can then be defined as:

$$Kn_{max,x} = \max_r[Kn_{max}(r,x)] \tag{5}$$

Fig. 7a shows how $Kn_{max,x}$ varies with x/L for the four different studied cases. Here, we defined L as the length of the divergent and x = 0 at the throat, where the maximum local Knudsen number reaches values between $Kn_{max,x}$ = 0.03 and $Kn_{max,x}$ = 0.11, for cases 1 and 4 respectively.

For each of the four studied cases, we performed a large number of different hybrid simulations. In each of them, the cross-sectional interface between the (upstream) CFD domain and the (downstream) DSMC domain was put in a different location x_{int}, varying from $x_{int}/L \sim -0.4$ (*i.e.* almost halfway in the convergent, upstream from the throat) to $x_{int}/L \sim 0.8$ (*i.e.* in the divergent, far downstream from the throat). With the inflow boundary conditions at $x = x_{int}$ extracted from the full CFD solution, a DSMC solution was performed for the domain between the interface at $x = x_{int}$ and the nozzle exhaust at $x = L$.

The results from all hybrid simulations for each of the four cases were compared to the full DSMC solution for that same case. The accuracy of each hybrid solution was estimated comparing the exit velocity and pressure profiles, with those obtained in the full DSMC solution. With N grid points in the exit cross section (for both the full and the hybrid DSMC simulation), an area weighted root mean square error is defined as:

$$RMS_\phi = \sqrt{\frac{\sum_{i=1}^{N}(\phi_{DSMC_i} - \phi_{Hyb_i})^2 A_i}{\sum_{i=1}^{N} A_i}} \tag{6}$$

This error was then normalized with the area weighted average difference between the exit end the inlet profiles of the full DSMC solution

$$\phi_{ref} = \sqrt{\frac{\sum_{i=1}^{N}(\phi_{DSMC_{out}} - \phi_{DSMC_{in}})_i^2 A_i}{\sum_{i=1}^{N} A_i}} \tag{7}$$

leading to

$$\varepsilon_\phi = \frac{RMS_\phi}{\phi_{ref}} \tag{8}$$

Fig. 7b displays the error as defined in Eq. (8) for both pressure and velocity, as a function of the location x_{int}/L at which the interface between CFD and DSMC was located. It should thus be noted that each symbol in Fig. 7b represents a separate hybrid simula-

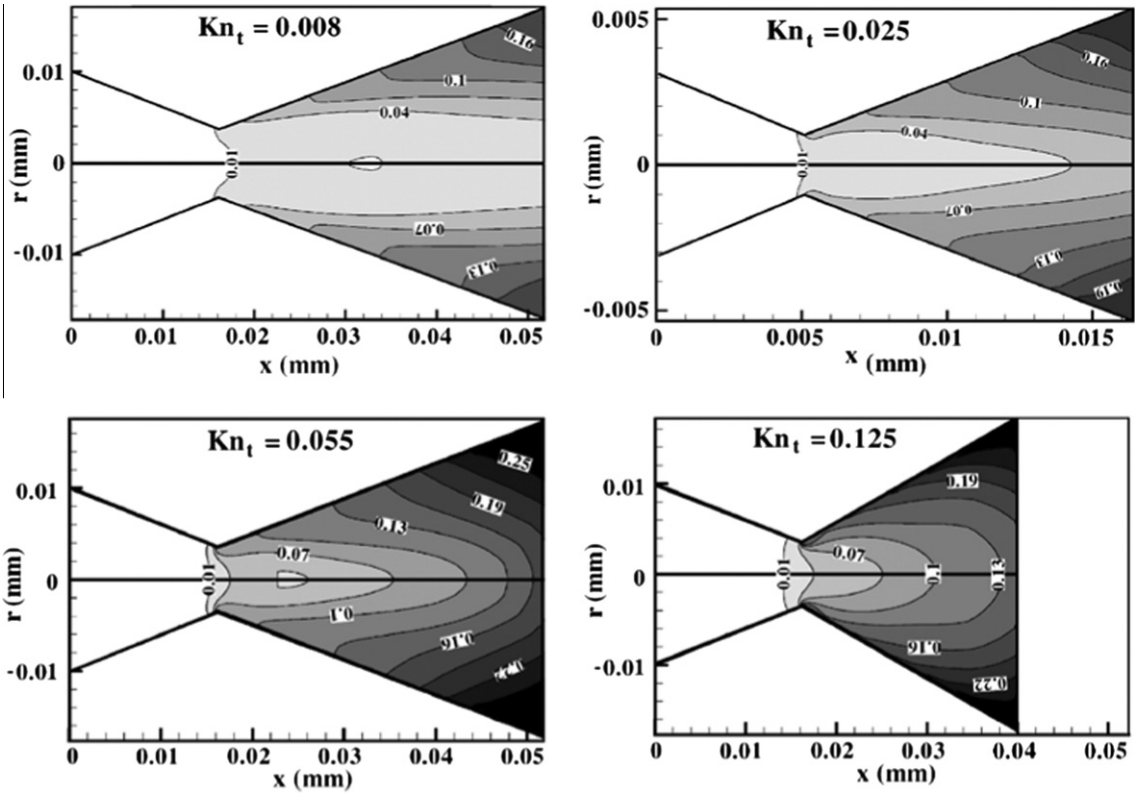

Fig. 6. Local maximum Knudsen number Kn_{max} computed from a full CFD simulation for the four considered configurations in Table 1.

tion, with the interface located at the corresponding x-coordinate. Similarly, Fig. 7c shows the error in the jet thrust and pressure thrust predicted by the hybrid simulations, normalized by the total thrust. For all four cases, the errors in the hybrid solution, as compared to the full DSMC solution, is small (below 2%) when the interface between CFD and DSMC is placed at an upstream, small x/L, location, before rarefaction starts to play a role. This clearly demonstrates, for the supersonic nozzle flows considered in this paper, the proper functioning of our coupling procedure between the upstream continuum simulations using the extended Fluent CFD solver, and the downstream DSMC simulations using the X-Stream/DSMC solver.

It can also be seen that, for each of the four studied cases, putting the interface location downstream from a certain critical location x/L leads to a rapid increase in the error for the hybrid simulation. Comparing Fig. 7a and b, it can be seen that the errors in the hybrid simulations, not surprisingly [13], start to increase rapidly when the interface is located at axial locations where the local maximum Knudsen number $Kn_{max,x}$ is larger than approximately 0.1, *i.e.* when CFD is applied in regions with local Knudsen numbers larger than 0.1.

For all the considered configurations we fitted the total square root error $\bar{\varepsilon} = \sqrt{\varepsilon_V^2 + \varepsilon_p^2}$, resulting from each simulation, with an exponential curve of the form $\bar{\varepsilon} = \varepsilon_0 + A\exp(Bx_{int})$. This is shown in Fig. 8. When the interface between CFD and DSMC is placed far upstream (small values of x_{int}), the error in the hybrid simulation, as compared to the full DSMC simulation, is some small base error ε_0, typically below 2%. When the interface is located further downstream, at larger x_{int}, the error increases. In the present study, the critical interface location $x_{int,crit}$ is defined as the value of x_{int} for which the curve fitted total error $\bar{\varepsilon}$ is twice the curve fitted base error ε_0.

The values of $x_{int,crit}$ for each of the four configurations are reported in Table 2, together with the corresponding maximum local Knudsen number for that location $Kn_{max,x}$. The results show that, as a rule of thumb, the location where $Kn_{max,x} \sim 0.1$ is the proper location for the interface between CFD and DSMC.

It is to be noted here, that the critical interface location does *not* generally coincide with the throat, as has been assumed in literature, *e.g.* in [19]. For case 1, the critical interface location is at $x/L \sim 0.46$, *i.e.* far downstream from the throat. For case 4, on the other hand, the critical interface location is at $x/L \sim -0.04$, *i.e.* a bit *upstream* from the throat. Putting the interface at a fixed location, *e.g.* at the throat, as was done in [19], may lead to inaccurate solutions for cases such as our case 4, in which rarefaction starts to play a role already before the throat, or to a waste of computational effort for cases such as our case 1, in which rarefaction starts to play a role only far downstream from the throat.

The latter is demonstrated in Fig. 7d, which shows the total CPU time required for the various hybrid simulations as a fraction of the CPU time required for a full DSMC simulation. For case 1, a hybrid simulation with the interface at the optimum location $x/L \sim 0.46$ can be performed in less than 5 % of the CPU time required for a full DSMC simulation. For the same case, putting the interface at the throat would increase the CPU time by a factor 3, at no significant gain in accuracy. For case 4, a hybrid simulation with the interface at the optimum location at $x/L \sim -0.04$ can be performed in less than 25% of the CPU time required for a full DSMC simulation. For the same case, putting the interface at the throat would decrease the CPU time by only a small fraction, at the cost of a rather significant decrease in accuracy.

The above discussion on accuracy focused on the accurate prediction of pressures and velocities in the nozzle exit. The situation changes if one is only interested in the accurate prediction of the *total thrust* T_{total}. Fig. 7b shows that the relative errors in the exit velocity and exit pressure have opposite signs. This is reflected in the errors in the predicted jet thrust and pressure thrust, as shown in Fig. 7c. When performing a hybrid CFD/DSMC simulation with

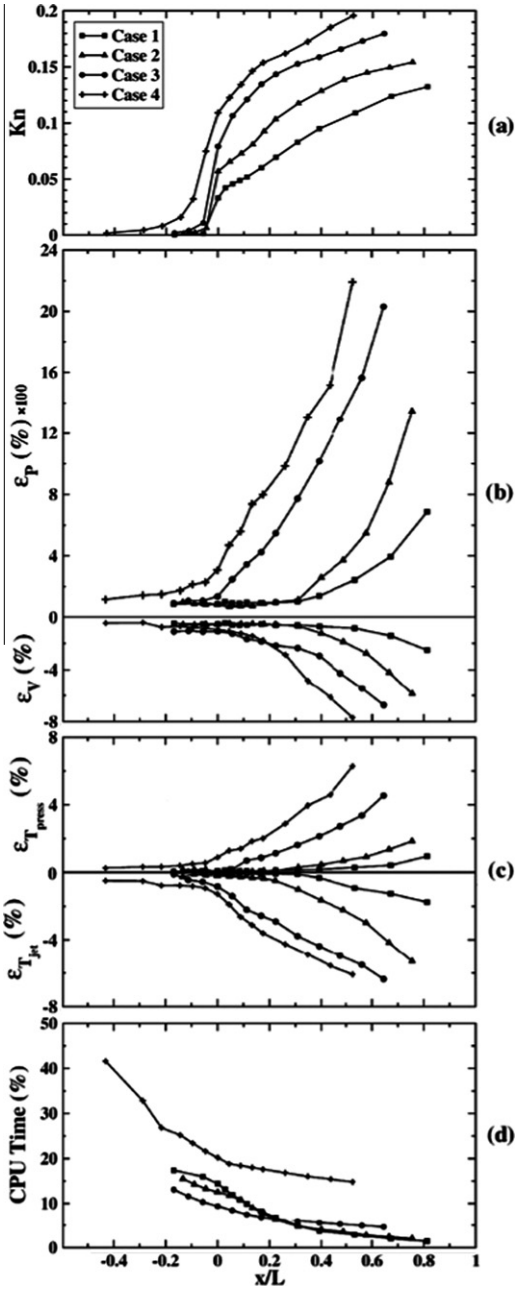

Fig. 7. For the four cases in Table 1: (a) local maximum cross sectional Knudsen number $Kn_{max,x}$ computed from a full CFD simulation, as a function of the dimensionless axial coordinate x/L; (b) relative difference in exit pressure and exit velocity between hybrid CFD/DSMC simulation with the interface located at x/L, and full DSMC simulation; (c) relative difference in jet thrust and pressure thrust between hybrid CFD/DSMC simulation with the interface located at x/L, and full DSMC simulation; (d) CPU time for hybrid CFD/DSMC simulation with the interface located at x/L, relative to the CPU time required for a full DSMC simulation.

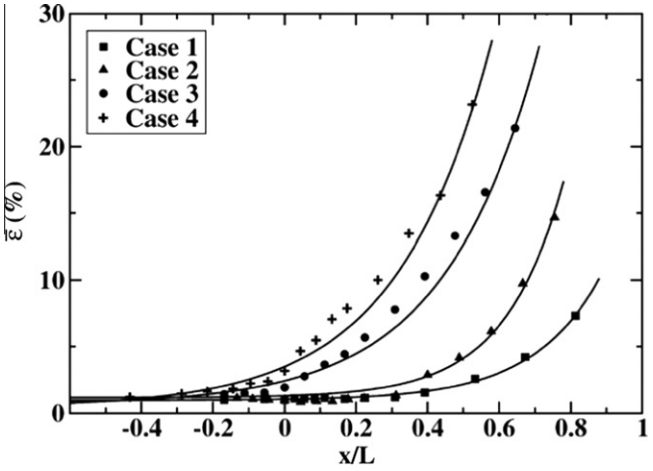

Fig. 8. For the four cases in Table 1 total square root error $\bar{\varepsilon}$, as a function of the dimensionless axial coordinate x/L and fitting exponential curves.

Table 2
Critical interface location $x_{int,crit}/L$ for which the total error $\bar{\varepsilon}$ equals twice the base error ε_0, and corresponding maximum local Knudsen number $Kn_{max,x}$.

Configuration	$x_{int,crit}/L$	$Kn_{max,x}$
1	0.461	0.102
2	0.304	0.116
3	0.038	0.103
4	−0.043	0.081

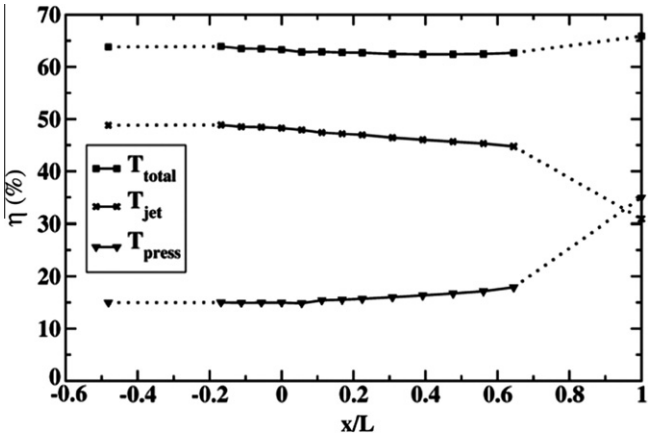

Fig. 9. Jet, pressure and overall nozzle efficiency for test case 3.

the interface located too far downstream, significant errors occur in the predicted jet trust and pressure thrust, but these errors almost entirely compensate each other. As a result, the error in the predicted total thrust remains very small (less than 1–2%).

This is further illustrated, for example, in Fig. 9 for case 3. Here the continuous lines connect the jet thrusts, pressure thrusts and overall thrusts as predicted by the hybrid simulations with interface locations varying from $-0.15 < x/L < 0.65$, relative to the total thrust predicted from 1D isentropic theory. Also shown are the jet thrust, pressure thrust and total thrust predicted by the full DSMC simulation (indicated by symbols at $x/L \sim -0.5$), and by the full CFD simulation with slip wall boundary condition (indicated by symbols at $x/L = 1$). Whereas for interface locations at $x/L > 0.1$ the individual errors in the predicted jet thrust and pressure thrust start to increase rapidly, the total predicted thrust is still within 2% accurate for the hybrid simulation with $x/L = 0.65$, and even for the full CFD simulation the error in the total thrust is less than 3%. It should also be noted that the total thrust predicted by DSMC, hybrid CFD/DSMC, and full CFD is in all cases significantly (*i.e.* 35%) lower than the thrust predicted by 1D isentropic theory.

5. Conclusions

In this paper we have shown that continuum based compressible CFD simulations, even when thermal and velocity slip at the walls are accounted for in the boundary conditions, cannot prop-

erly predict gas velocities and pressures in micro-nozzles with throat dimensions in the μm range, and thrusts in the μN range. We have performed accurate full DSMC simulations of four different micro-nozzles in this range, varying the throat Knudsen number from 0.008 to 0.125 by varying the throat diameter, divergent angle and inlet pressure. For all cases, even when the throat Knudsen number was below 0.01, full CFD simulations led to a significant over-prediction of the outlet pressure, and a significant under-prediction of the outlet velocities. In cases with throat Knudsen numbers of the order of 0.1, CFD even completely failed to predict a supersonic flow region, which was clearly present in the DSMC simulations.

On the other hand, we have shown that accurate flow and pressure simulations can be obtained with hybrid CFD/DSMC simulations, applying a simple, static, state-based, one-way coupling between a commercial CFD solver used upstream from a certain cross-sectional interface, and a commercial DSMC solver used downstream from that interface. When the location of the interface is chosen properly, hybrid simulations require only 5–25% of full DSMC simulations, whereas predicted outflow pressures and velocities differ less than 1–2%.

The optimum location of the cross-sectional interface plane was shown to not generally coincide with the plane of the throat, but to lay upstream or downstream from the throat, depending on the flow conditions. It was shown that the optimum location of the interface can be predicted *a priori* from local Knudsen numbers based on gradient length scales of pressure, density and temperature, as calculated from a full CFD simulation of the entire nozzle. The interface should be placed at the cross section where the maximum local Knudsen number starts to exceed 0.1.

A bit surprisingly, it was found that full CFD simulations of micro-nozzles with μN thrusts, as well as inaccurate hybrid CFD/DSMC simulations of such nozzles, do quite a good job in predicting the overall thrust. Application of a continuum CFD solver in regions were rarefaction is important leads to an over-prediction of the nozzle outlet pressure (and therefore of its pressure thrust), and an under-prediction of the nozzle outlet velocity (and therefore of its jet thrust). The two effects almost perfectly compensate, leading to overall thrust predictions within 3% of the total thrust predicted by full DSMC and accurate hybrid CFD/DSMC simulations.

The overall thrust predicted by all numerical schemes was found to be several tens of percents lower than the thrust predicted by 1D isentropic flow theory.

Acknowledgement

This work was funded by MicroNed, one of the Dutch BSIK (Besluit Subsidies Investeringen Kennisinfrastructuur) research programs.

References

[1] Moerel JLPA, Sanders HM, Louwerse MC, Jansen HV, Boscher J, Zandbergen BTC et al. Development of micro propulsion system technologies for minisatellites in the Netherlands. In: Saccoccia G, Amand P-G, editors. Proc of 5th international spacecraft propulsion conference and 2nd international symposium on propulsion for space transportation, Crete, Greece, 5–8 May 2008.

[2] Zandbergen BCT, Louwerse MC, Tardaguila F, Koopmans RJ, Boscher J, Moerel JPLA. Initial development of a miniature cold gas propulsion system for nano/microsatellites.' In: Saccoccia G, Amand P-G, editors. Proc of 5th international spacecraft propulsion conference and 2nd international symposium on propulsion for space transportation, Crete, Greece, 5–8 May 2008.

[3] La Torre F, Kenjeres S, Moerel JLPA, Zandbergen BTC, Kleijn CR. Influence of boundary layer formation and surface roughness on the thrust of micro-nozzle. In: Saccoccia G, Amand P-G, editors. Proc of 5th international spacecraft propulsion conference and 2nd international symposium on propulsion for space transportation, Crete, Greece, 5–8 May 2008.

[4] Sutton GP, Biblarz O. Rocket propulsion elements. John Wiley& Sons; 2001.

[5] La Torre F, Kenjeres S, Kleijn CR, Moerel JLPA. Effects of wavy surface roughness on the performance of micronozzles. J Propul Power 2010;26(4):655–62.

[6] Liu M, Zhang X, Zhang G, Chen Y. Study on micronozzle flow and propulsion performance using DSMC and continuum methods. Acta Mech Sin 2006;22:409–16.

[7] Markelov GN, Ivanov MS, Ketsdever AD, Wadsworth DC. Numerical study of cold gas micronozzle flows. In: Proc 33th aerospace science meeting and exhibit, AIAA 99-0166; 1999.

[8] Gadepalli VVV, Lin C. Navier–Stokes modeling of gas flows in a de-laval micronozzle. In: Proc 44th AIAA aerospace sciences meeting and exhibit, AIAA 2006-1425; 2006.

[9] Mo H, Lin C, Gokaltun S, Skudarnov PV. Numerical study of axisymmetric gas flow in conical micronozzle by DSMC and continuum methods. In: Proc 44th AIAA aerospace sciences meeting and exhibit, AIAA 2006-991; 2006.

[10] Titov EV, Kumar R, Levin DA, Gimelshein NE, Gimelshein SF. Analysis of different approaches to modeling of nozzle flows in the near continuum regime. In: Proc 26th rarefied gas dynamics int symposium, AIP conf proc, 1084; 2009. p. 978–84.

[11] Cercignani C. The Boltzmann equation and its applications. Springer Verlag; 1988.

[12] Hadjiconstantinou NG. Comment on Cercignanis second-order slip coefficient. Phys Fluids 2003;15:2352.

[13] Bird GA. Molecular gas dynamics and the direct simulation of gas flows. Oxford: Oxford Science Publ.; 1994.

[14] Boyd ID, Penko PF, Meissner DL, DeWitt KJ. Experimental and numerical investigations of low-density nozzle and plume flows of nitrogen. AIAA J 1992;30(10):2453–61.

[15] Xie C. Characteristics of micronozzle gas flows. Phys Fluids 2007;19(3).

[16] Markelov GN, Ivanov MS. Numerical study of 2D/3D micronozzle flows. In: Proc 22nd rarefied gas dynamics int symposium. AI P conf proc, vol. 585; 2001. p. 539–46.

[17] Buoni M, Kietz D, Aslam K, Subramaniam VV. Simulation of a compressible gas flow in a micronozzle. In: Proceedings 35th AIAA thermophysics conf, AIAA 2001-3073; 2001.

[18] Alexenko AA, Collins RJ, Gimelshein SF, Levin DA. Challenges of three-dimensional modeling of microscale propulsion devices with the DSMC method. In: Proc 22nd rarefied gas dynamics int symposium, AIP conf proc, vol. 585; 2001. p. 464–71.

[19] Alexenko AA, Levin DA, Gimelshein SF, Collins RJ. Numerical modeling of axisymmetric and three-dimensional flows in MEMS nozzle. AIAA J 2002;40(5):897–904.

[20] Wu ZN, Xu SS, Gao B, Zhuang LS. Review of numerical computation of compressible flows with artificial interfaces. Comput Fluids 2007;36:1657–79.

[21] Wijesinghe HS, Hadjiconstantinou NG. Discussion of hybrid atomistic-continuum methods for multiscale hydrodynamics. Int J Multiscale Comput Eng 2004;2:189–202.

[22] Aktas O, Aluru NR. A combined continuum/DSMC technique for multiscale analysis of microfluidic filters. J Comput Phys 2002;178(2):342–72.

[23] Roveda R, Goldstein DB, Varghese PL. Hybrid Euler/particle approach for continuum/rarefied flows. J Spacecraft Rockets 1998;35(3):258–65.

[24] Roveda R, Goldstein DB, Varghese PL. Hybrid Euler/direct simulation Monte Carlo calculation of unsteady slit flow. J Spacecraft Rockets 2000;37(6):753–60.

[25] Wijesinghe HS, Hornung RD, Garcia AL, Hadjiconstantinou NG. Three-dimensional continuum-atomistic simulations for multiscale hydrodynamics. J Fluids Eng 2004;126(5):768–76.

[26] Garcia AL, Bell JB, Crutcheld WY, Alder BJ. Adaptive mesh and algorithm refinement using direct simulation Monte Carlo. J Comput Phys 1999;154(1):134–55.

[27] Glass CE, Gnoffo PA. A 3D coupled CFD–DSMC solution method with application to the mars sample return orbiter. NASA Langley Research Center TR NASA-2000-22isrgd-ceg, Hampton; 2000.

[28] Schwartzentruber TE, Scalabrin LC, Boyd ID. Hybrid particle-continuum simulations of non-equilibrium hypersonic blunt body flowfields. J Thermophys Heat Transfer 2008;22(1):29–37.

[29] Schwartzentruber TE, Boyd ID. A hybrid particle-continuum method applied to shock waves. J Comput Phys 2006;215:402–16.

[30] Carlson A, Roveda R, Boyd ID, Candler GV. A hybrid CFD–DSMC method of modeling continuum-rareed flows. 42nd AIAA aerospace sciences meeting and exhibit, AIAA paper 2004-1180; 2004.

[31] Schwartzentruber TE, Scalabrin LC, Boyd ID. A modular particle-continuum method for hypersonic non-equilibrium gas flows. J Comput Phys 2007;225:1159–74.

[32] Abbate G, Kleijn CR, Thijsse BJ. Hybrid continuum/molecular simulations of transient gas flows with rarefaction. AIAA J 2009;47(7):1741–9.

[33] Hadjiconstantinou NG, Garcia AL, Bazant MZ, He G. Statistical error in particle simulations of hydrodynamic phenomena. J Comput Phys 2003;187:274–97.

[34] Glass CE, Horvarth TJ. Comparison of a 3-D CFD–DSMC solution methodology with a wind tunnel experiment. NASA TM-2002-211777; 2002.

[35] Xu SS, Wu ZN, Li Q, Hong YJ. Hybrid continuum/DSMC computation of rocket mode lightcraft flow in near space with high temperature and rarefaction effect. Comput Fluids 2009;38(7):1394–404.

[36] Abbate G, Kleijn CR, Thijsse BJ, Engeln R, Sanden MCM, Schram DC. Influence of rarefaction on the flow dynamics of a stationary supersonic hot-gas expansion. Phys Rev E 2008;77(3).

[37] Boyd ID, Chen G, Chandler GV. Predicting failure of the continuum fluid equations in transitional hypersonic flows. Phys Fluids 1995;7(1):210–9.
[38] FLUENT 6 Tutorial Guide. FLUENT Inc., Natick, MA; 2005.
[39] Hirschfelder JO, Curtis CF, Bird RB. Molecular theory of gasses and liquids. Wiley; 1954.
[40] Maxwell JC. On stresses in rarefied gases arising from inequalities of temperature. Filos Trans Roy Soc Lond 1879;170:231.
[41] von Smoluchowski M. Über wärmeleitung in verdünnten gasen. Ann Phys Chem 1898;64:101–30.
[42] Sharipov F, Seleznev V. Data on internal rarefied gas flows. J Phys Chem Ref Data 1998;27:657–707.
[43] Sharipov F. Application of the Cercignani Lampis scattering kernel to calculations of rarefied gas flows. II. Slip and jump coefficients. Eur J Mech B: Fluids 2003;22:657–69.
[44] Gambit 2 Tutorial Guide. FLUENT Inc., Natick, MA; 2001.
[45] CVD-X User Manual. The Netherlands Organization for Applied Scientific Research TNO & Femsys Ltd., Eindhoven; 2007.
[46] Dorsman R. Numerical simulations of rarefied gas flows in thin film processes. PhD thesis, Delft; 2007.
[47] Alexander FJ, Garcia AL, Alder BJ. Cell size dependence of transport coefficients in stochastic particle algorithms. Phys Fluids 1998;10(6):1540–2.
[48] Hadjiconstantinou NG. Analysis of discretization in the direct simulation Monte Carlo. Phys Fluids 2002;12(10):2634–8.
[49] Ilgaz M, Celenligil MC. DSMC simulations of low-density choked flows in parallel-plate channels. In: Proc 23rd rarefied gas dynamics int symposium. AIP conf proc, vol. 663; 2003. p. 831–8.
[50] Rader DJ, Gallis MA, Torczynski JR, Wagner W. DSMC convergence behaviour for fourier flow. In: Proc 24th rarefied gas dynamics int symposium. AIP conf proc, vol. 762; 2005. p. 473–8.
[51] Bird GA. The DS2V/3V program suite for DSMC calculations. In: Proc 24th rarefied gas dynamics int symposium. AIP conf proc, vol. 762; 2005. p. 541–6.
[52] Gallis MA, Torczynski JR, Rader DJ, Bird GA. Accuracy and convergence of a new DSMC algorithm. American Institute of Aeronautics and Astronautics paper no. AIAA 2008-3913; 2008.
[53] La Torre F, Kenjeres S, Kleijn CR, Moerel JLPA. Evaluation of micronozzle performance through DSMC, Navier–Stokes and coupled DSMC/Navier–Stokes approaches. Lecture notes in computer science, vol. 5544. Los Angeles: Springer; 2009. p. 675–84.
[54] Hamel BB, Willis DR. Kinetic theory of source flow expansion with application to the free jet. Phys Fluids 1966;9:829–41.
[55] Wang WL, Boyd ID. Predicting continuum breakdown in hypersonic viscous flows. Phys Fluids 2003;15(1):91–100.
[56] Bird GA. Breakdown of translational and rotational equilibrium in gaseous expansions. Am Inst Aero Astro J 1970;8.
[57] Garcia AL, Bell JB, Crutchfield WY, Alder BJ. Adaptive mesh and algorithm refinement using direct simulation Monte Carlo. J Comput Phys 1999;154:134.
[58] Hash DB, Hassan HA. Assessment of schemes for coupling Monte Carlo and Navier–Stokes solution methods. J Thermophys Heat Transfer 1996;10(2):242–9.
[59] Vashchenkov PV, Kudryavtsev AN, Khotyanovsky DV, Ivanov MS. DSMC and Navier–Stokes study of backflow for nozzle plumes expanding into vacuum. In: Proc 24th rarefied gas dynamics int symposium. AIP conf proc, vol. 762; 2005. p. 355–9.
[60] Wu J-S, Lian Y-Y, Cheng G, Koomullil RP, Tseng K-C. Development and verification of a coupled DSMC-NS scheme using unstructured mesh. J Comput Phys 2006;219:579–607.
[61] Schwartzentruber TE, Scalabrin LC, Boyd ID. Hybrid particle-continuum simulations of hypersonic flow over a hollow-cylinder-flare geometry. AIAA J 2008;46(8):2086–95.
[62] Tiwari S, Klar A, Hardt S. A particle–particle hybrid method for kinetic and continuum equations. J Comput Phys 2009;228:7109–24.
[63] John B, Damodaran M. Computation of head-disk interface gap micro flowfields using DSMC and continuum-atomistic hybrid methods. Int J Numer Methods Fluids 2009;61:1273–98.
[64] Donev A, Bell JB, Garcia AL, Alder BJ. A hybrid particle-continuum method for hydrodynamics of complex fluids. Multiscale Mod Simul 2010;8(3):871–911.
[65] Wadsworth DC, Erwin DA. Two-dimensional hybrid continuum/particle approach for rarefied flows. In: AI AA 23rd plasmadynamics & lasers conference AIAA-92-2975; 1992. p. 1–7.